12-1-2008

Analyzing the Catalytic Role of Asp97 in the Methionine Aminopeptidase from *Escherichia coli*

Sanghamitra Mitra
Utah State University

Kathleen M. Job
Utah State University

Lu Meng
Utah State University

Brian Bennett
Marquette University, brian.bennett@marquette.edu

Richard C. Holz
Marquette University, richard.holz@marquette.edu

Accepted version. *FEBS Journal,* Vol. 275, No. 24 (December 2008): 6248-6259. DOI.
Brian Bennett was affiliated with the Medical College of Wisconsin at the time of publication.
Richard C. Holz was affiliated with Loyola University-Chicago at the time of publication.

Analyzing The Catalytic Role of Asp97 in The Methionine Aminopeptidase from *Escherichia coli*

Sanghamitra Mitra
Department of Chemistry and Biochemistry,
Utah State University,
Logan, UT
Kathleen M. Job
Department of Chemistry and Biochemistry,
Utah State University,
Logan, UT
Lu Meng
Department of Chemistry and Biochemistry,
Utah State University,
Logan, UT
Brian Bennett
Department of Biophysics, National Biomedical EPR Center,
Medical College of Wisconsin,
Milwaukee, WI

FEBS Journal, Vol. 275, No. 24 (December 2008): pg. 6248-6259. DOI.

Richard C. Holz

Department of Chemistry and Biochemistry,
Utah State University,
Logan, UT
Department of Chemistry, Loyola University-Chicago,
Chicago, IL

Abstract: An active site aspartate residue, Asp97, in the methionine aminopeptidase (MetAPs) from *Escherichia coli* (*Ec*MetAP-I) was mutated to alanine, glutamate, and asparagine. Asp97 is the lone carboxylate residue bound to the crystallographically determined second metal-binding site in *Ec*MetAP-I. These mutant *Ec*MetAP-I enzymes have been kinetically and spectroscopically characterized. Inductively coupled plasma–atomic emission spectroscopy analysis revealed that 1.0 ± 0.1 equivalents of cobalt were associated with each of the Asp97-mutated *Ec*MetAP-Is. The effect on activity after altering Asp97 to alanine, glutamate or asparagine is, in general, due to a ~ 9000-fold decrease in k_{ca} towards Met-Gly-Met-Met as compared to the wild-type enzyme. The Co(II) *d–d* spectra for wild-type, D97E and D97A *Ec*MetAP-I exhibited very little difference in form, in each case, between the monocobalt(II) and dicobalt(II) *Ec*MetAP-I, and only a doubling of intensity was observed upon addition of a second Co(II) ion. In contrast, the electronic absorption spectra of [Co_(D97N *Ec*MetAP-I)] and [CoCo(D97N *Ec*MetAP-I)] were distinct, as were the EPR spectra. On the basis of the observed molar absorptivities, the Co(II) ions binding to the D97E, D97A and D97N *Ec*MetAP-I active sites are pentacoordinate. Combination of these data suggests that mutating the only nonbridging ligand in the second divalent metal-binding site in MetAPs to an alanine, which effectively removes the ability of the enzyme to form a dinuclear site, provides a MetAP enzyme that retains catalytic activity, albeit at extremely low levels. Although mononuclear MetAPs are active, the physiologically relevant form of the enzyme is probably dinuclear, given that the majority of the data reported to date are consistent with weak cooperative binding.

Keywords: EPR, kinetics, mechanism, methionine aminopeptidases, mutants

Methionine aminopeptidases (MetAPs) represent a unique class of protease that is responsible for the hydrolytic removal of N-terminal methionines from proteins and polypeptides [1–4]. In the cytosol of eukaryotes, all proteins are initiated with an N-terminal methionine; however, all proteins synthesized in prokaryotes, mitochondria and chloroplasts are initiated with an N-terminal formylmethionyl that is subsequently removed by a deformylase, leaving a free methionine at

FEBS Journal, Vol. 275, No. 24 (December 2008): pg. 6248-6259. DOI.

the N-terminus [2]. The cleavage of this N-terminal methionine by MetAPs plays a central role in protein synthesis and maturation [5,6]. The physiological importance of MetAP activity is underscored by the cellular lethality upon deletion of the MetAP genes in *Escherichia coli, Salmonella typhimurium*, and *Saccharomyces cerevisiae* [7–10]. Moreover, a MetAP from eukaryotes has been identified as the molecular target for the antiangiogenesis drugs ovalicin and fumagillin [11–15]. Therefore, the inhibition of MetAP activity in malignant tumors is critical in preventing tumor vascularization, which leads to the growth and proliferation of carcinoma cells. In comparison to conventional chemotherapy, antiangiogenic therapy has a number of advantages, including low cellular toxicity and a lack of drug resistance [14].

MetAPs are organized into two classes (type I and type II) on the basis of the absence or presence of an extra 62 amino acid sequence (of unknown function) inserted near the catalytic domain of type II enzymes. The type I MetAPs from *E. coli* (*Ec*MetAP-I), *Staphylococcus aureus, Thermotoga maritima* and *Homo sapiens* and the type II MetAPs from *Homo sapiens* and *Pyrococcus furiosus* (*Pf*MetAP-II) have been crystallographically characterized [14,16–21]. All six display a novel 'pita-bread' fold with an internal pseudo-two-fold symmetry that structurally relates the first and second halves of the polypeptide chain to each other. Each half contains an antiparallel β-pleated sheet flanked by two helical segments and a C-terminal loop. Both domains contribute conserved residues as ligands to the divalent metal ions residing in the active site. Nearly all of the available X-ray crystallographic data reported to date reveal a bis(μ-carboxylato) (μ-aquo/hydroxo) dinuclear core with an additional carboxylate residue at each metal site and a single histidine bound to M1 (Fig. 1) [22,23]. However, extended X-ray absorption fine structure spectroscopy (EXAFS) studies on Co(II)- and Fe(II)-loaded *Ec*MetAP-I did not reveal any evidence for a dinuclear site [23]. An X-ray crystal structure of *Ec*MetAP-I was recently reported with partial occupancy (40%) of a single Mn(II) ion bound in the active site [24]. This structure was obtained by adding the transition state analog inhibitor l-norleucine phosphonate, in order to impede divalent metal binding to the second site, and by limiting the amount of metal ion present during crystal growth. This structure provides the first structural verification that MetAPs can form mononuclear active sites and that the single divalent

FEBS Journal, Vol. 275, No. 24 (December 2008): pg. 6248-6259. DOI.

metal ion resides on the His171 side of the active site, as previously predicted by ^{1}H-NMR spectroscopy and EXAFS [22,23].

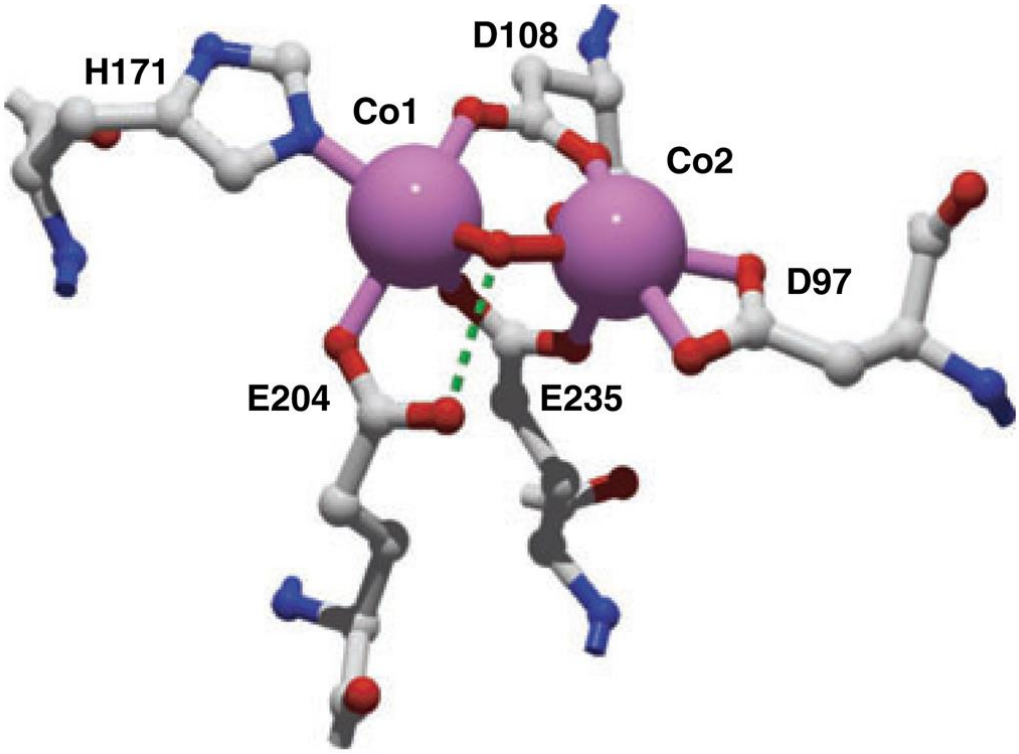

Fig. 1: Active site of *Ec*MetAP-I showing the metal-binding residues, including Asp97. Prepared from Protein Data Bank file 2MAT.

A major controversy currently surrounding MetAPs is whether a mononuclear site, a dinuclear site or both can catalyze the cleavage of N-terminal methionines *in vivo* [22,25,26]. A growing number of kinetic studies indicate that both type I and type II MetAPs are fully active in the presence of only one equivalent (eq.) of divalent metal ion [Mn(II), Fe(II), or Co(II)] [22,25,27]. However, kinetic, magnetic CD (MCD) and atomic absorption spectrometry data indicated that Co(II) ions bind to *Ec*MetAP-I in a weakly cooperative fashion (Hill coefficients of 1.3 or 2.1) [26,28]. These data represent the first evidence that a dinuclear site can form in *Ec*MetAP-I under physiological conditions. Moreover, EPR data recorded on Mn(II)-loaded *Ec*MetAP-I and *Pf*MetAP-II suggest a small amount of dinuclear site formation after the addition of only a quarter equivalent of Mn(II) [22,29,30]. In order to determine whether a dinuclear site is required for enzymatic activity in MetAPs, the conserved aspartate, which is the

lone nonbridging ligand for the M2 site in MetAPs (Fig. 2), was mutated in *Ec*MetAP-I to alanine, glutamate, and asparagine.

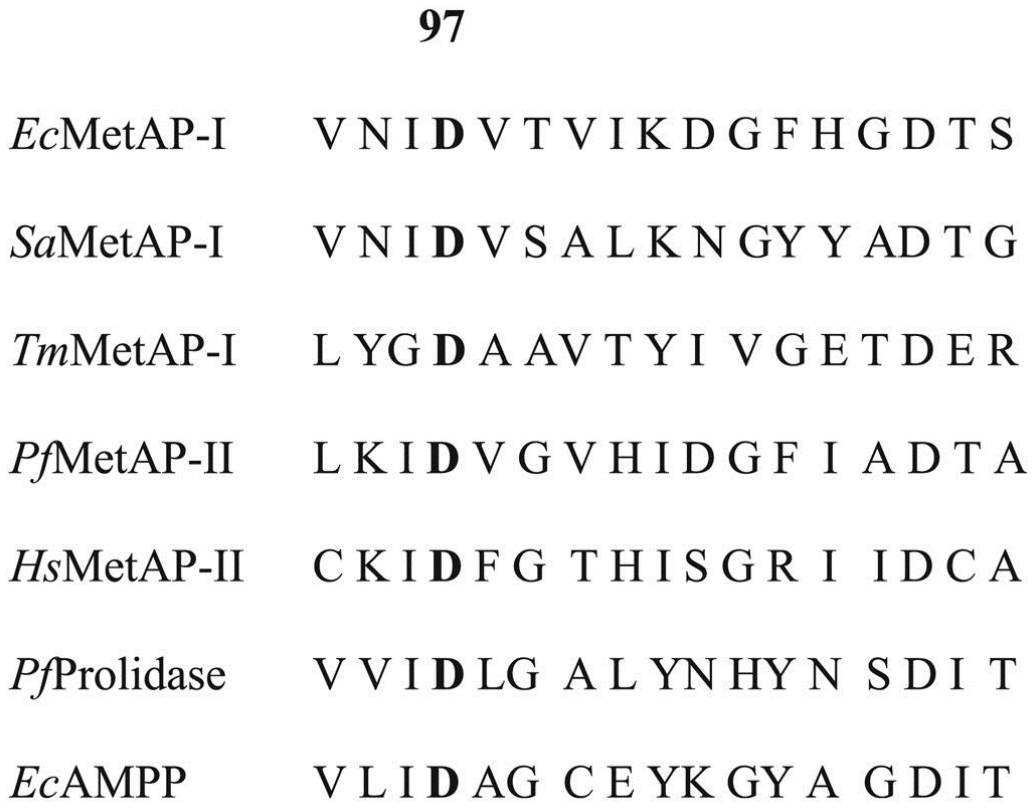

Fig. 2: Amino acid sequence alignment for selected MetAPs, prolidase and aminopeptidase P (AMPP). Prepared from Protein Data Bank files 1C21, 1QXZ, 1O0X, 1XGO, 1BN5, 1PV9, and 1A16.

Results

Metal content of mutant EcMetAP-I enzymes

The number of tightly bound divalent metal ions was determined for each of the mutant *Ec*MetAP-I enzymes by inductively coupled plasma–atomic emission spectroscopy (ICP-AES) analysis. Apoenzyme samples (30 μm), to which 2–30 eq. of Co(II) were added under anaerobic conditions, were dialyzed for 3 h at 4 °C with Chelex-100-treated, metal-free Hepes buffer (25 mm Hepes, 150 mm KCl, pH 7.5). ICP-AES analysis revealed that 1.0 ± 0.1 eq. of cobalt was associated with each of the Asp97-mutated *Ec*MetAP-I enzymes. As a control, metal analyses were also performed on the corresponding

Asp82 mutant *Pf*MetAP-II enzymes. ICP-AES analysis of D82A, D82N and D82E *Pf*MetAP-II also revealed that 1.0 ± 0.1 eq. of cobalt was associated with the enzymes.

Kinetic analysis of the mutant EcMetAP-I enzymes

The specific activities of D97A, D97N and D97E *Ec*MetAP-I were examined using Met-Gly-Met-Met (MGMM) as the substrate. Apo-forms of the variants were all catalytically inactive. Kinetic parameters were determined for the Co(II)-reconstituted wild-type and mutated enzymes (Table 1). In order to obtain detectable activity levels, reactions of D97A, D97N and D97E *Ec*MetAP-I with MGMM were allowed to run for > 24 h before quenching of the reactions, as compared to 1 min for wild-type *Ec*MetAP-I. The extent of the reaction for the variants was obtained from the time dependence of the activity of the enzymes. A linear correlation was observed between activity and time until 30 h, after which the activity values reached a plateau. As a control, substrate was incubated with apo-*Ec*MetAP-I and in buffer, neither of which resulted in any observed substrate cleavage. All three variants exhibited maximum catalytic activity after the addition of only one equivalent of Co(II), which is identical to what was found with wild-type *Ec*MetAP-I [22,31].

Table 1: Kinetic parameters for Co(II)-loaded wild-type (WT) and D97 mutated *Ec*MetAP-I towards MGMM at 30 °C and pH 7.5. SA, specific activity.

	EcMetAP-I			
	WT	**D97A**	**D97N**	**D97E**
K_m (mm)	3.0 ± 0.1	1.1 ± 0.1	0.6 ± 0.1	1.8 ± 0.1
k_{cat} (s^{-1})	18.3 ± 0.5	0.003 ± 0.001	0.001 ± 0.0005	0.002 ± 0.001
k_{cat} / K_m ($m^{-1}{\cdot}s^{-1}$)	6.0×10^3	3.0	2.0	1.0
SA (units·mg^{-1})	36.1 ± 2	0.006 ± 0.001	0.002 ± 0.001	0.004 ± 0.001

The effect on activity after altering Asp97 to alanine, glutamate or asparagine is, in general, due to a decrease in k_{cat}. The k_{cat} values for D97A, D97E and D97N *Ec*MetAP-I are 0.003 ± 0.001, 0.002 ± 0.001, and 0.001 ± 0.0005 s^{-1}, respectively (Table 1). Thus, the k_{cat} value for the variants towards MGMM decreased ~ 9000-fold as compared to the wild-type enzyme. For comparison purposes, k_{cat} values of D82E, D82N and D82A *Pf*MetAP-II were determined, and

FEBS Journal, Vol. 275, No. 24 (December 2008): pg. 6248-6259. DOI.

were found to be 10 ± 1, 1.4 ± 0.1, and 0.01 ± 0.005 s^{-1}, respectively. Thus, the k_{cat} value for D82A *Pf*MetAP-II towards MGMM decreased ~ 19 000-fold as compared to wild-type *Pf*MetAP-II, whereas D82E *Pf*MetAP-II was only 19-fold less active. As a control, we also altered the *Pf*MetAP-II active site histidine (His153), which is analogous to His171 in *Ec*MetAP-I, to an alanine. This mutation, not surprisingly, resulted in the complete loss of enzymatic activity. Moreover, this enzyme does not bind divalent metal ions, as determined by ICP-AES analysis. These data clearly establish His153 (His171) as an essential active site amino acid involved in metal binding.

The K_m values for each of D97A, D97E and D97N *Ec*MetAP-I decreased in comparison to that of wild-type *Ec*MetAP-I, with the largest drop in K_m being observed for D97N *Ec*MetAP-I (0.6 ± 0.1 mm), which contains the most conservative substitution. The observed K_m value for D97E *Ec*MetAP-I was 1.8 ± 0.1 mm, whereas D97A *Ec*MetAP-I exhibited a K_m value of 1.1 ± 0.1 mm. Combination of the observed k_{cat} and K_m values for each *Ec*MetAP-I variant provided the catalytic efficiency (k_{cat}/K_m) for the Co(II)-loaded enzymes, which was decreased 2000-fold, 6100-fold and 3000-fold for D97A, D97E and D97N *Ec*MetAP-I, respectively, towards MGMM. In order to confirm the accuracy of the K_m values, the dissociation constant (K_d) for MGMM binding to Co(II)-loaded D97N *Ec*MetAP-I was determined by isothermal calorimetry (ITC) and found to be 0.9 mm, which is similar in magnitude to the observed K_m value.

Determination of metal-binding constants

ITC measurements were carried out at 25 ± 0.2 °C for D97E, D97A and D97N *Ec*MetAP-I (Fig. 3). Association constants (K_a) for the binding of Co(II) were obtained by fitting these data, after subtraction of the background heat of dilution, via an iterative process using the origin software package. This software package uses a nonlinear least-square algorithm that allows the concentrations of the titrant and the sample to be fitted to the heat-flow-per-injection to an equilibrium binding equation for two sets of noninteracting sites. The K_a value, the metal–enzyme stoichiometry (p) and the change in enthalpy ($\Delta H°$) were allowed to vary during the fitting process (Table 2, Fig. 3). The

FEBS Journal, Vol. 275, No. 24 (December 2008): pg. 6248-6259. DOI.

best fit obtained for D97A *Ec*MetAP-I provided an overall *p*-value of 2 for two noninteracting sites, whereas the best fit obtained for D97N *Ec*MetAP-I provided an overall *p*-value of 3 for three noninteracting sites. Similarly, the best fit obtained for D97E *Ec*MetAP-I provided an overall *p*-value of 3 for three interacting sites. For D97A *Ec*MetAP-I, K_d values of 1.6 ± 1.2 μm and 2.2 ± 0.4 mm were observed, whereas D97N *Ec*MetAP-I gave a K_d value of 0.22 ± 0.3 μm and two K_d values of 0.2 ± 0.1 mm. Interestingly, D97E *Ec*MetAP-I exhibited cooperative binding, giving K_d values of 90 ± 20, 210 ± 100 and 574 ± 150 μm. The heat of reaction, measured during the experiment, was converted into other thermodynamic parameters using the Gibbs free energy relationship. The thermodynamic parameters obtained from ITC titrations of Co(II) with wild-type *Ec*MetAP-I and each mutant enzyme reveal changes that affect both of the metal-binding sites (Table 3). Although the predominant effect is on the second metal-binding site, substitution of Asp97 by glutamate and asparagine makes the process of binding of the metal ions, particularly for the second metal ion, more spontaneous on the basis of more negative Gibbs free energy (ΔG) values in comparison to the wild-type enzyme. Substitution of Asp97 by alanine does not affect the ΔG value for the binding of the first metal ion; however, the entropic factor ($T\Delta S$) for the binding of the first metal ion decreases in the relative order D97E > wild type > D97N > D97A. In addition, $T\Delta S$ for binding of the second metal ion significantly decreases for D97N *Ec*MetAP-I but remains similar in magnitude for D97E *Ec*MetAP-I in comparison to the wild-type enzyme.

FEBS Journal, Vol. 275, No. 24 (December 2008): pg. 6248-6259. DOI.

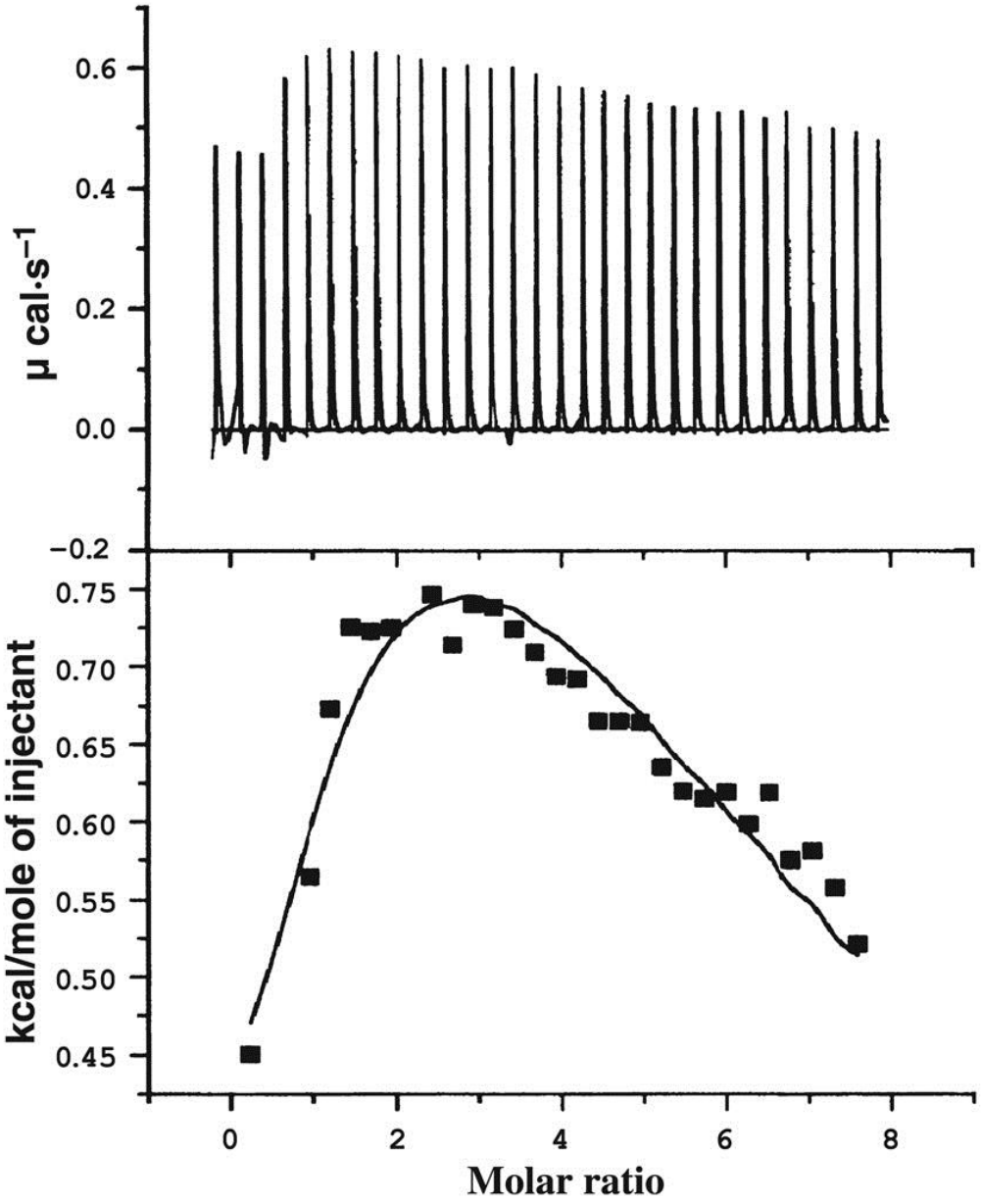

Fig. 3: ITC titration of 70 μm solution of D97E *Ec*MetAP-I with a 5 mm Co(II) solution at 25 °C in 25 mm Hepes (pH 7.5) and 150 mm KCl.

***Ec*MetAP-I**	***p***	K_{d1}, K_{d2} **(μm)**
WT	1	1.6 ± 0.5
	2	14 000 ± 5000
D97A	1	1.6 ± 1.2
	1	2237 ± 476
D97N	1	0.22 ± 0.3
	2	238 ± 100
D97E	1	90 ± 20
	1	210 ± 100
	1	574 ± 150

Table 2: Dissociation constants (K_d) and metal–enzyme stoichiometry (n) for Co(II) binding to wild-type (WT) and variant *Ec*MetAP-I. For each set of data for both WT and variant *Ec*MetAP-I, p is the number of Co(II) ions per protein. Data for p = 1 are for one Co(II) ion that bound tightly, and data for p = 2 represent two Co(II) ions binding to sites on the protein with lower affinity. WT data have been reported in [49].

***Ec*MetAP-I**	***p***	ΔH_1, ΔH_2 **(kcal / mol)**	$T\Delta S_1$,$T\Delta S_2$ **(kcal·mol^{-1})**	ΔG_1, ΔG_2 **(kcal·mol^{-1})**
WT	1	1.54×10^{1}	2.33×10^{1}	−7.91
	2	1.06×10^{3}	1.06×10^{3}	−2.51
D97A	1	1.42×10^{0}	9.35×10^{0}	−7.90
	1	1.64×10^{1}	2.00×10^{1}	−3.61
D97N	1	1.40×10^{0}	1.05×10^{1}	−9.07
	2	4.20×10^{0}	9.14×10^{0}	−4.94
D97E	1	6.31×10^{-1}	8.12×10^{3}	−5.49
	1	5.03×10^{0}	10.02×10^{3}	−4.99
	1	6.20×10^{0}	10.60×10^{3}	−4.40

Table 3: Thermodynamic parameters for Co(II) binding to wild-type (WT) and variant *Ec*MetAP-I.

Electronic absorption spectra of Co(II)-loaded mutated EcMetAP-I

The electronic absorption spectra of wild-type, D97A, D97N and D97E *Ec*MetAP-I with the addition of one and two equivalents of Co(II) were recorded under strict anaerobic conditions in 25 mm Hepes buffer (pH 7.5) and 150 mm KCl (Fig. 4). The addition of one equivalent of Co(II) to wild-type, D97A, D97N and D97E *Ec*MetAP-I provided electronic absorption spectra with three absorption maxima between 540 and 700 nm, with molar absorptivities ranging from 20 to 80 $m^{-1}·cm^{-1}$. In general, the addition of a second equivalent of Co(II) increased the molar absortivities of the absorption bands. However, for D97N *Ec*MetAP-I, molar absorptivity increased for maxima at 550 and

FEBS Journal, Vol. 275, No. 24 (December 2008): pg. 6248-6259. DOI.

630 nm but diminished for the maxima at 690 nm (Fig. 4). Addition of further equivalents of Co(II) led to precipitation for D97N *Ec*MetAP-I, no change in molar absorptivity of the absorption maxima for D97A *Ec*MetAP-I, but an increase in molar absorptivity for D97E *Ec*MetAP-I.

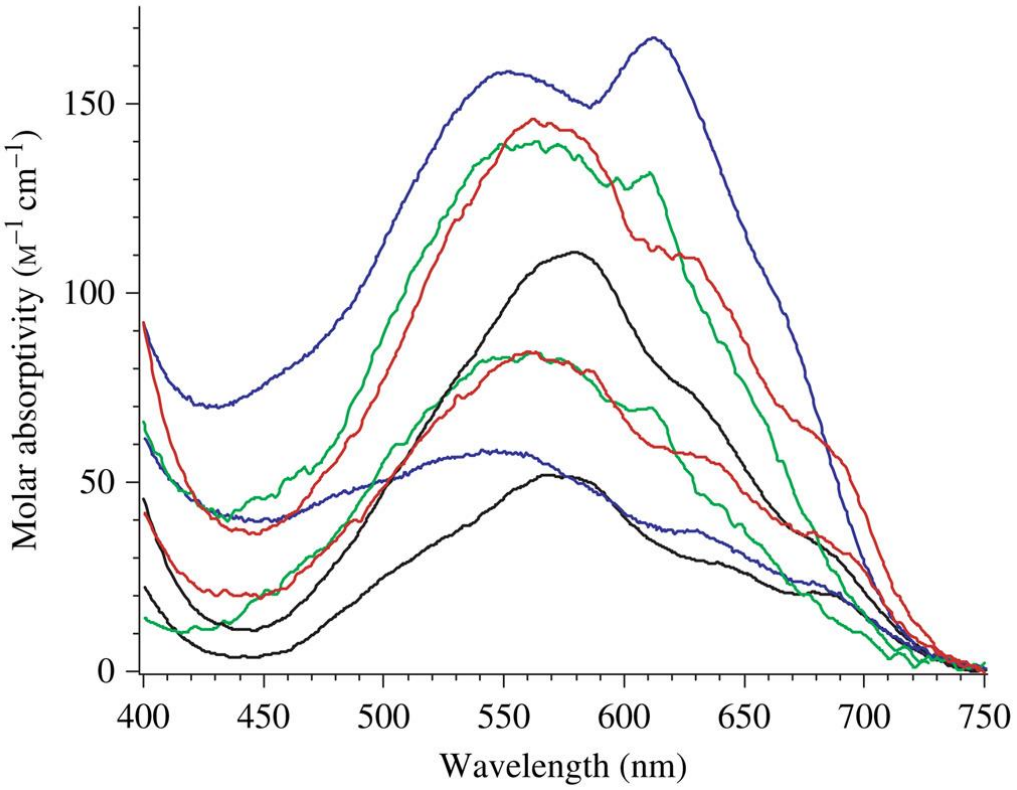

Fig. 4: Electronic absorption spectra of 1 mm wild-type (black), D97A (green), D97N (blue) and D97E (red) *Ec*MetAP-I with increments of one and two equivalents of Co(II) in 25 mm Hepes buffer (pH 7.5) and 150 mm KCl.

For D97E *Ec*MetAP-I, the dissociation constant for the second metal-binding site was determined by subtraction of the UV–visible spectrum with one equivalent of Co(II) from the other spectra and then plotting a binding curve (Fig. 5). The dissociation constants (K_d) for the second divalent metal-binding sites of *Ec*MetAP-I D97E were obtained by fitting the observed molar absorptivities to Eqn (1), via an iterative process that allows both K_d and p to vary (Fig. 5):

$$r = pC_S/(K_d + C_S) \quad (1)$$

FEBS Journal, Vol. 275, No. 24 (December 2008): pg. 6248-6259. DOI.

where p is the number of sites for which interaction with M(II) is governed by the intrinsic dissociation constant K_d, and r is the binding function calculated by conversion of the fractional saturation (f_a) [32]:

$$r = f_a p \tag{2}$$

C_S, the free metal concentration, was calculated from

$$C_S = C_{TS} - rC_A \tag{3}$$

where C_{TS} and C_A are the total molar concentrations of metal and enzyme, respectively. The best fit obtained for the λ_{max} values at 520, 627 and 685 nm provided a P-value of 1 and K_d values of 0.3 ± 0.1, 1.1 ± 0.2 and 0.6 ± 0.6 mm, respectively, for D97E *Ec*MetAP-I (Table 4).

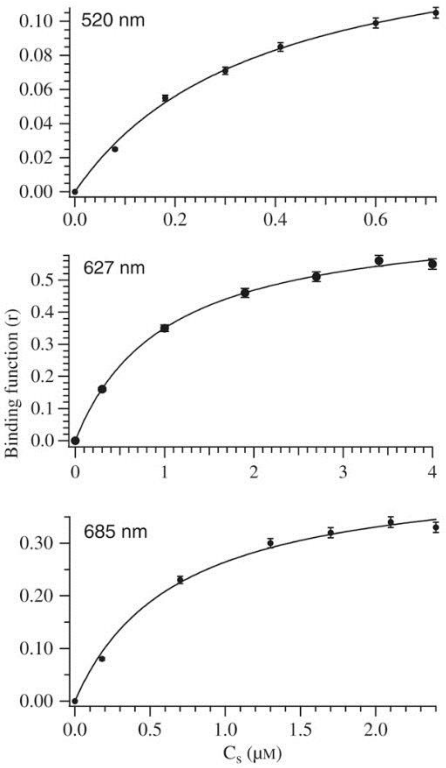

Fig. 5: Binding function r versus C_S, the concentration of free metal ions in solution for D97E *Ec*MetAP-I in 25 mm Hepes buffer (pH 7.5) and 150 mm KCl at three different wavelengths. The solid lines correspond to fits of each data set to Eqn (3).

FEBS Journal, Vol. 275, No. 24 (December 2008): pg. 6248-6259. DOI.

λ_{max} (nm)	K_d (mm)
520	0.3 ± 0.1
627	1.1 ± 0.2
685	0.6 ± 0.6

Table 4: Data obtained for the fits of electronic absorption data to Eqn (1).

EPR studies of Co(II)-loaded D97A, D97E and D97N EcMetAP-I

The EPR spectrum of wild-type *Ec*MetAP-I (Fig. 6A) has been well characterized [22], and the form of the signal is invariant from 0.5 to 2.0 eq. of Co(II). The signal is due to transitions in the M_S = | ± 1/2⟩ Kramers' doublet of S = 3/2, with Δ > $g\beta BS$, and exhibits no resolved rhombicity or ^{59}Co hyperfine structure. This type of signal is typical for protein-bound five- or six-coordinate Co(II) with one or more water ligands. A very similar signal was obtained with the mono-Co(II) form of D97A *Ec*MetAP-I (Fig. 6K) and with the di-Co(II) forms of both D97A (Fig. 6L) and D97N (Fig. 6H,J) *Ec*MetAP-I.

FEBS Journal, Vol. 275, No. 24 (December 2008): pg. 6248-6259. DOI.

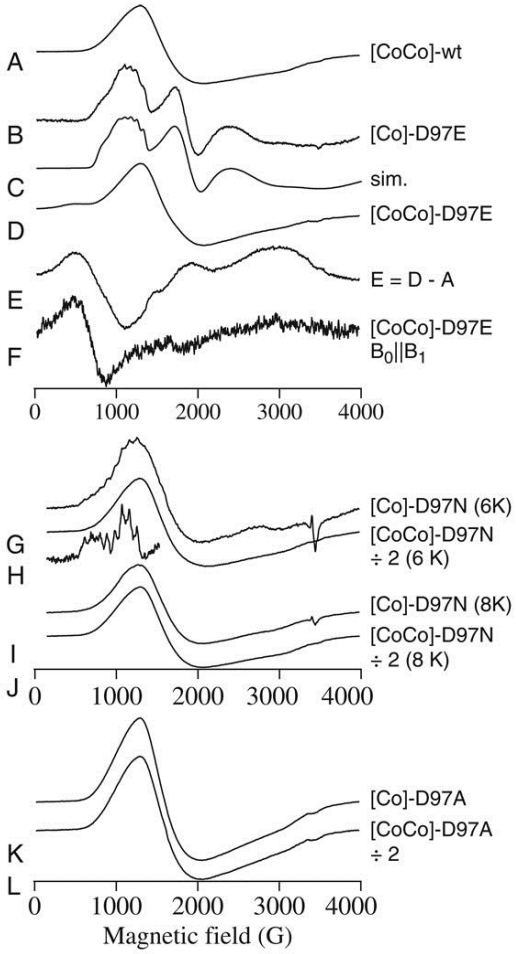

Fig. 6
Co(II)-EPR of *Ec*MetAP-I and variants. Traces A, B and D are the EPR spectra of [CoCo(WT-*Ec*MetAP-I)] (A), [Co_(D97E-*Ec*MetAP-I)] (B), and [CoCo(D97E-*Ec*MetAP-I)] (D). Trace C is a computer simulation of B assuming two species. The major species exhibited resolved hyperfine coupling and was simulated with spin Hamiltonian parameters $S = 3/2$, $M_S = |\pm 1/2\rangle$, $g_{x,y} = 2.57$, $g_z = 2.67$, $D >> g\,BS$ (50 cm-1), $E/D = 0.185$, $A_y = 9.0 \times 10^{-3}$ cm^{-1}. The minor species was best simulated ($g_{x,y} = 2.18$, $g_z = 2.6$, $E/D = 1/3$, A_y (unresolved) $= 4.5 \times 10^{-3}$ cm^{-1}) assuming some unresolved hyperfine coupling, although no direct evidence for this was obtained. Trace E is of spectrum D with arbitrary amounts of spectrum A subtracted. Trace F is the experimental EPR spectrum of [CoCo(D97E- *Ec*MetAP-I)] recorded in parallel mode ($B_0 \parallel B_1$). Traces G and I are spectra of [Co_(D97N- *Ec*MetAP-I)], and traces H and J are spectra of [CoCo(D97N- *Ec*MetAP-I)]; the insert of H shows the hyperfine region of G expanded. Trace K is the spectrum of [Co_(D97A- *Ec*MetAP-I)], and L is of [CoCo(D97A-*Ec*MetAP-I)]. Spectra A, B, D and I–K were recorded using 0.2 mW power at 8 K. Spectrum F was recorded using 20 mW at 8 K, and spectra G and H were recorded using 2 mW at 6 K. Trace G is shown × 2 compared to H, I is shown × 2 compared to J, and K is shown × 2 compared to L. Other intensities are arbitrary. Spectrum F was recorded at 9.37 GHz whereas all other experimental spectra were at 9.64 GHz.

FEBS Journal, Vol. 275, No. 24 (December 2008): pg. 6248-6259. DOI.

The EPR signals from D97E *Ec*MetAP-I were, however, significantly different from those of wild-type *Ec*MetAP-I. The signal observed for [Co_(D97E *Ec*MetAP-I)] (Fig. 6B) was complex, and computer simulation (Fig. 6C) suggested a dominant species that exhibited marked rhombic distortion of the axial zero-field splitting (E/D = 0.185) and a ^{59}Co hyperfine interaction of 9×10^{-3} cm^{-1}. These parameters are typical for low-symmetry five-coordinate Co(II) with a constrained ligand sphere, and suggest that either Co(II) is displaced relative to that in [Co_(wild-type *Ec*MetAP-I)] and binds in a very different manner altogether, or that the binding mode of the carboxylate differs, perhaps being bidentate in D97E *Ec*MetAP-I and replacing a water ligand. Further differences between the binding modes of Co(II) were observed in the dicobalt(II) form of D97E *Ec*MetAP-I. Whereas there was no evidence for significant exchange coupling in spectra obtained for wild-type *Ec*MetAP-I, the spectrum of [CoCo(D97E *Ec*MetAP-I)] (Fig. 6D) exhibited a feature at $g_{eff} \sim 12$ that was suggestive of an integer spin system with $S' = 3$. Subtraction of the [Co_(D97E *Ec*MetAP-I)] spectrum and the wild-type spectrum yielded a difference spectrum (Fig. 6E) with similarities to integer spin signals observed in other dicobalt(II) systems [33], and the parallel mode EPR signal, with a resonance at $g_{eff} \sim 11$ (Fig. 6F), confirmed that the Co(II) ions in [CoCo(D97E *Ec*MetAP-I)] do indeed form a weakly exchange-coupled dinuclear center.

Close examination of the EPR signal from [Co_(D97N *Ec*MetAP-I)] recorded at 6 K (Fig. 6G) revealed a ^{59}Co hyperfine pattern superimposed on the dominant axial signal, indicating the presence of two species of Co(II). The pattern was centered at $g_{eff} \sim 7.9$ and, interestingly, no other features that could be readily associated with this pattern were evident. It is possible, then, that the hyperfine pattern in the spectrum of [Co_(D97N *Ec*MetAP-I)] is part of an $M_S = |\pm 3/2\rangle$ signal, indicative of tetrahedral character for Co(II) ions, for which the $g_\perp$ features are unobservable at 9.6 GHz. This explanation is also consistent with the loss of the hyperfine pattern upon an increase of the temperature by a mere 2 K; $M_S = |\pm 3/2\rangle$ signals are often only observed at temperatures around 5 K, because of rapid relaxation at higher temperatures [34–36]. Despite the superficial similarity of the hyperfine patterns observed in the spectra of [Co_(D97N *Ec*MetAP-I)] and [Co_(D97E *Ec*MetAP-I)], the Co(II) species from which these originate are probably very different. An additional difference between

FEBS Journal, Vol. 275, No. 24 (December 2008): pg. 6248-6259. DOI.

D97N and D97E *Ec*MetAP-I is the lack of evidence for exchange coupling in [CoCo(D97N *Ec*MetAP-I)]; the formation of a spin-coupled dinuclear center appears to be unique to D97E *Ec*MetAP-I.

Discussion

A major stumbling block in the design of small molecule inhibitors of MetAPs centers on how many metal ions are present in the active site under physiological conditions. Most of the X-ray crystallographic data reported for MetAPs indicate that two metal ions form a dinuclear active site [24,37–42]. However, kinetic data suggest that only one metal ion is required for full enzymatic activity, and EXAFS studies on Co(II)-and Fe(II)-loaded *Ec*MetAP-I did not provide any evidence for a dinuclear site [22,23,25,27]. Recently, the X-ray crystal structure of a mono-Mn(II) *Ec*MetAP-I enzyme bound by l-norleucine phosphonate was reported, providing the first crystallographic data for a mononuclear MetAP [24]. Taken together, these data suggest that MetAPs are mononuclear exopeptidases, however, kinetic, MCD and atomic absorption spectrometry data indicate that Co(II) ions bind to *Ec*MetAP-I in a weakly cooperative fashion [26,28]. In order to reconcile these data and determine whether a dinuclear site is required for enzymatic activity, as well as shed some light on the catalytic role of Asp97 in *Ec*MetAP-I, we prepared the D97A, D97E and D97N mutant enzymes. This aspartate is strictly conserved in all MetAPs as well as in other enzymes in the 'pita-bread' superfamily (e.g. aminopeptidase P and prolidase) (Fig. 2) [14,16,17,19,21,43–46]. Replacement of this conserved aspartate in human prolidase by asparagine causes skin abnormalities, recurrent infections, and mental retardation [45].

On the basis of ICP-AES analyses, both D97A *Ec*MetAP-I and D82A *Pf*MetAP-II bind only one divalent metal ion tightly, which is identical to what is seen with the wild-type enzyme [22,25]. Therefore, the second metal ion is either not present or is loosely associated. Consistent with ICP-AES analyses, the K_d value determined for D97A *Ec*MetAP-I using ITC indicates the presence of only one tightly bound divalent metal ion, and the K_{d1} is not affected as compared to the wild-type enzyme [22,25]. Therefore, the K_{d1} value observed for D97A *Ec*MetAP-I appears to correspond to the microscopic binding constant

FEBS Journal, Vol. 275, No. 24 (December 2008): pg. 6248-6259. DOI.

of a single metal ion to the histidine-containing side of the *Ec*MetAP-I active site, consistent with the hypothesis that substitution of Asp97, a residue that functions as the only nonbridging ligand for the second metal-binding site, effectively eliminates the ability of a second divalent metal ion to bind in the active site. For wild-type *Ec*MetAP-I, two additional weak metal-binding events are also observed. Rather than three total observed metal-binding sites, D97A *Ec*MetAP-I binds only two Co(II) ions, the second probably being in a remote Co(II)-binding site identified in the X-ray crystal structure of *Ec*MetAP-I [15,19]. This remote metal-binding site, or third metal-binding site, was also observed in the structure of the type I methionine aminopeptidase from *H. sapiens* [21]. In both enzymes, this remote site is on the outer edge of the enzyme and becomes at least partially occupied at Co(II) concentrations near 1 mm. Therefore, the second divalent metal-binding event observed via ITC for D97A *Ec*MetAP-I is postulated to be due to the binding of a Co(II) ion to the remote divalent metal-binding site with a K_{d2} of 2.2 mm.

ICP-AES data obtained with D97N and D97E *Ec*MetAP-I are also consistent with ITC data, in that only one tightly bound divalent metal ion is present in these enzymes. Interestingly, the ITC data obtained for D97E Ec*MetAP-I* can only be fitted on the assumption of positive cooperativity, similar to that reported by Larrabee *et al.* for wild-type *Ec*MetAP-I [26]. The enhanced cooperativity observed for D97E versus wild-type *Ec*MetAP-I is probably due to the increased carbon chain length of glutamate versus aspartate, which may adjust the position of the second metal-binding site. Similar to what is seen with wild-type *Ec*MetAP-I, two weak binding events are also observed for D97N and D97E *Ec*MetAP-I, suggesting that a second metal ion can still bind to the dinuclear active site even when the bidentate ligand aspartate is replaced by glutamate or asparagine. However, the ability of D97N and D97E *Ec*MetAP-I to bind a second divalent metal ion increases ~ 60-fold as compared to wild-type *Ec*MetAP-I.

The observed k_{cat} values for D97A *Ec*MetAP-I in the presence of three equivalents of Co(II) at pH 7.5 decreased 6100-fold as compared to the wild-type enzyme. D97N and D97E *Ec*MetAP-I are also slightly active, but neither of these mutant enzymes recover wild-type activity levels. These data are consistent with a previous study on D97A *Ec*MetAP-I, where it was reported that ~ 4% of the residual activity of

FEBS Journal, Vol. 275, No. 24 (December 2008): pg. 6248-6259. DOI.

wild-type *Ec*MetAP-I was retained [47]. On the basis of these data, this strictly conserved aspartate is a catalytically important residue but is not absolutely required for enzymatic activity. The fact that catalytic activity is observed for both D97A *Ec*MetAP-I and D82A *Pf*MetAP-II, enzymes in which the second divalent metal-binding site has probably been eliminated, suggests that MetAP enzymes can function as mononuclear enzymes. Interestingly, the observed K_m value for D97A *Ec*MetAP-I, which is a partial indicator of the affinity of an enzyme for its substrate, decreased by ~ 2.7-fold, suggesting that D97A *Ec*MetAP-I binds MGMM more tightly than the wild-type enzyme. The combination of these data provides a catalytic efficiency for D97A *Ec*MetAP-I that is ~ 4000-fold poorer than that of wild-type *Ec*MetAP-I. This result is significant in light of the evidence that metal binding to D97A *Ec*MetAP-I is probably not cooperative and dinuclear sites do not appear to form.

Further insight into the structure–function relationships of the metal-binding sites of *Ec*MetAP-I comes from electronic absorption and EPR spectroscopy. The Co(II) *d–d* spectra for wild-type, D97E and D97A *Ec*MetAP-I exhibited very little difference in form, in each case, between the monocobalt(II) and dicobalt(II) forms, and only a doubling of intensity was observed upon addition of a second Co(II) ion. For wild-type and D97A *Ec*MetAP-I, this was reflected in the EPR spectra, which also did not differ significantly between the monocobalt(II) and dicobalt(II) forms. In contrast, the electronic absorption spectra of [Co_(D97N *Ec*MetAP-I)] and [CoCo(D97N *Ec*MetAP-I)] are distinct, as are the EPR spectra. On the basis of the observed molar absorptivities, the Co(II) ions binding to the D97E, D97A and D97N *Ec*MetAP-I active sites are pentacoordinate [48] and, apart from a putative tetrahedral species implied by a minor component of the EPR spectrum of [Co_(D97N *Ec*MetAP-I)], the EPR spectra are all consistent with this interpretation, with high axial symmetry being seen in D97A and D97N *Ec*MetAP-I. The minor component in D97N *Ec*MetAP-I that is tentatively assigned as a tetrahedral Co(II) may be in equilibrium (in solution) with the dominant five-coordinate form, and the EPR signal due to this species was not exhibited by the dicobalt(II) form of D97N *Ec*MetAP-I. This, in turn, suggests that rearrangement of the active site upon binding a second Co(II) ion leads to a preference for the higher coordination geometry, perhaps due to stabilization of a hitherto weakly bound

water ligand by either bridging the two Co(II) ions or via hydrogen bonding.

EPR spectra obtained for D97E *Ec*MetAP-I are particularly interesting, and indicate: (a) a much more distorted five-coordinate geometry for the first Co(II) ion with a much more rigid ligand complement, which probably lacks a solvent ligand; and (b) the formation of a weakly exchange-coupled *bona fide* dinuclear site upon the addition of two Co(II) ions. Taken together, the EPR data obtained for D97E *Ec*MetAP-I suggest that the loss of aspartate at position 97 is not responsible for the observed change in the Co(II) environment of the M1 site, but rather the presence of the glutamate side chain. It is tempting to speculate that Glu97 provides one or more ligands to the first Co(II)-binding site, and indeed bidentate binding of Glu97 may prevent binding of the solvent ligand that appears to be present in other mono-cobalt(II) species of *Ec*MetAP-I.

Combination of these data suggests that mutating the only nonbridging ligand in the second divalent metal-binding site in MetAPs to an alanine, which effectively removes the ability of the enzyme to form a dinuclear site, provides a MetAP enzyme that retains catalytic activity, albeit at extremely low levels. Reconciliation of these data with kinetic, ITC, crystallographic and EXAFS data suggesting that MetAPs are mononuclear with kinetic, MCD and EPR data indicating that metal binding is cooperative, at first glance, appears to be tricky [22,24,26,29,30]. However, the most logical explanation leads to the conclusion that metal binding to MetAPs is cooperative, and that discrepancies have arisen due to the concentrations of the enzyme samples used in the various experiments. For example, ITC data do not reveal cooperative binding for divalent metal ions to *Ec*MetAP-I or *Pf*MetAP-II but, instead, indicate that one metal ion binds with much higher affinity than subsequent metal ions. It should be noted that ITC titrations are typically run with enzyme concentrations of 70 μm, and most often reveal two sets of binding sites, similar to that observed for D97N *Ec*MetAP-I [22]. Likewise, initial activity assays carried out on *Ec*MetAP-I and *Pf*MetAP-II used an enzyme concentration of 20 μm, which is two orders of magnitude larger than the K_d value determined for the first metal-binding site of 0.2 or 0.4 μm, assuming Hill coefficients of 1.3 or 2.1, respectively [26,28]. However, a K_d value of between 2.5 and 4.0 μm was reported if it was assumed that only a

FEBS Journal, Vol. 275, No. 24 (December 2008): pg. 6248-6259. DOI.

single Co(II)-binding site exists in the low-concentration regime, which is within the error of ITC and kinetic K_d values. Spectroscopic and most X-ray crystallographic measurements were carried out at much higher enzyme (~ 1 mm) and metal concentrations, where a significant concentration of dinuclear sites will undoubtedly be present. Under the conditions utilized in ITC experiments, any cooperativity in divalent metal binding will not be detectable, but may appear in EPR and electronic absorption data. As activity titrations and ITC data are not particularly sensitive to the type of binding (i.e. cooperativity versus two independent binding sites), the weak cooperativity observed by Larrabee *et al.* [26] will not be observed in these experiments but is entirely consistent with the EPR and electronic absorption data and, indeed, with recent X-ray crystallographic data. Most X-ray structures of MetAPs were determined with a large excess of divalent metal ions, so only dinuclear sites were observed. However, crystallographic data obtained on *Ec*MetAP-I using metal ion / enzyme ratios of 0.5 : 1 reveal metal ion occupancies of 71% bound to the M1 site and 28% bound to the M2 site, consistent with cooperative binding [24].

In conclusion, mutating the only nonbridging ligand in the second divalent metal-binding site in MetAPs to an alanine, which effectively removes the ability of the enzyme to form a dinuclear site, provides MetAPs that retain catalytic activity, albeit at extremely low levels. Although mononuclear MetAPs are active, the physiologically relevant form of the enzyme is probably dinuclear, given that the majority of the data reported to date are consistent with weak cooperative binding. Therefore, Asp97 primarily functions as a ligand for the second divalent metal-binding site, but also probably assists in binding and positioning the substrate through interactions with the N-terminal amine. The data reported herein highlight the complexity of the active site of *Ec*MetAP-I, and provide additional insights into the role that active site residues play in the hydrolysis of peptides by MetAPs as well as aminopeptidase P and prolidase.

FEBS Journal, Vol. 275, No. 24 (December 2008): pg. 6248-6259. DOI.

Experimental procedures

Mutagenesis, protein expression and purification

Altered forms of *Ec*MetAP-I were obtained by PCR mutagenesis using the following primers: 5′-GGC GAT ATC GTT AAC ATT XXX GTC ACC GTA ATC AAA GAT GG-3′ and 5′-CCA TCT TTG ATT ACG GTG AC YYY A ATG TTA ACG ATA TCG CC-3′, with XXX standing for GCT, AAT, or GAG, and YYY standing for AGC, TTA, or CTC, of *Ec*MetAP-I D97A, D97N and D97E. Site-directed mutants were obtained using the Quick Change Site-Directed Mutagenesis Kit (Stratagene, La Jolla, CA, USA), following Stratagene's procedure. Reaction products were transformed into *E. coli* XL1-Blue competent cells (*recA1 endA1 gyrA96 thi-1 hsdR17 supE44 relA1 lac [F′ proAB lacI*^{q}*ZΔ M15 Tn10*(*Tet*^{r})]), grown on LB agar plates containing kanamycin at a concentration of 50 μg·mL^{-1}. A single colony of each mutant was grown in 50 mL of LB containing 50 μg·mL^{-1} kanamycin. Plasmids were isolated using Wizard Plus Miniprep DNA purification kits (Promega, Madison, WI, USA) or Qiaprep Spin Miniprep kits (Qiagene, Valencia, CA, USA). Each mutation was confirmed by DNA sequencing (USU Biotechnology Center). Plasmids containing the altered *Ec*MetAP-I genes were transformed into *E. coli* BL21 Star(DE3) [*F*$^{-}$ *ompT hsdS*$_B$ (*r*$_B$ $^{-}$*m*$_B$ $^{-}$) *gal* dcm *rne131* (DE3)] (Invitrogen, Carlsbad, CA, USA), and stock cultures were prepared. The variants were purified in an identical manner to the wild-type enzyme [15,31]. Purified variants exhibited a single band on SDS /PAGE at an *M*^{r} of 29 630. Protein concentrations were estimated from the absorbance at 280 nm using an extinction coefficient of 16 445 m^{-1}·cm^{-1} [12,18]. Apo-*Ec*MetAP-I was washed free of methionine using Chelex-100-treated methionine-free buffer (25 mm Hepes, pH 7.5, 150 mm KCl) and concentrated by microfiltration using a Centricon-10 (Amicon, Beverly, MA, USA) prior to all kinetic assays. Individual aliquots of apo-*Ec*MetAP-I were routinely stored at −80 °C or in liquid nitrogen until needed. Similarly, we also prepared D82E, D82N and D82A *Pf*MetAP-II and purified them to homogeneity, according to SDS /PAGE analysis.

FEBS Journal, Vol. 275, No. 24 (December 2008): pg. 6248-6259. DOI.

Metal content measurements

Mutated *Ec*MetAP-I enzyme samples prepared for metal analysis were typically 30 μm. Apo-*Ec*MetAP-I samples were incubated anaerobically with MCl_2, where M = Co(II), for 30 min prior to exhaustive anaerobic exchange into Chelex-100-treated buffer as previously reported [31]. Metal analyses were performed using ICP-AES.

Enzymatic assay of EcMetAP-I enzymes

All enzymatic assays were performed under strict anaerobic conditions in an inert atmosphere glove box (Coy) with a dry bath incubator to maintain the temperature at 30 °C. Catalytic activities were determined with an error of ± 5%. Enzyme activities for each mutated enzyme were determined in 25 mm Hepes buffer (pH 7.5) containing 150 mm KCl with the tetrapeptide substrate MGMM. The amount of product formation was determined by HPLC (Shimadzu LC-10A class-VP5). A typical assay involved the addition of 8 μL of metal-loaded *Ec*MetAP-I enzyme to a 32 μL substrate–buffer mixture at 30 °C for 1 min. The reaction was quenched by the addition of 40 μL of a 1% trifluoroacetic acid solution. Elution of the product was monitored at 215 nm following separation on a C8 HPLC column (Phenomenex, Luna; 5 μm, 4.6 × 25 cm), as previously described [22,31]. Enzyme activities are expressed as units per milligram, where one unit is defined as the amount of enzyme that releases 1 μmol of product in 1 min at 30 °C.

ITC

ITC measurements were carried out on a MicroCal OMEGA ultrasensitive titration calorimeter. The titrant ($CoCl_2$) and apo-*Ec*MetAP-I solutions of the mutated enzymes were prepared in Chelex-100-treated 25 mm Hepes buffer at pH 7.5, containing 150 mm KCl. Stock buffer solutions were thoroughly degassed before each titration. The enzyme solution (70 μm) was placed in the calorimeter cell and stirred at 200 r.p.m. to ensure rapid mixing. Typically, 3 μL of titrant was delivered over 7.6 s with a 5-min interval between injections to allow for complete equilibration. Each titration was continued until

FEBS Journal, Vol. 275, No. 24 (December 2008): pg. 6248-6259. DOI.

4.5–6 eq. of Co(II) had been added, to ensure that no additional complexes were formed in excess titrant. A background titration, consisting of the identical titrant solution but only the buffer solution in the sample cell, was subtracted from each experimental titration to account for heat of dilution. These data were analyzed with a two- or three-site binding model by the Windows-based origin software package supplied by MicroCal [49].

Spectroscopic measurements

Electronic absorption spectra were recorded on a Shimadzu UV-3101PC spectrophotometer. All variant apo-*Ec*MetAP-I samples used in spectroscopic measurements were made rigorously anaerobic prior to incubation with Co(II) ($CoCl_2$, ≥ 99.999%; Strem Chemicals, Newburyport, MA) for ~ 30 min at 25 °C. Co(II)-containing samples were handled throughout in an anaerobic glove box (Ar /5% H_2, ≤ 1 p.p.m. O_2; Coy Laboratories) until frozen. Electronic absorption spectra were normalized for the protein concentration and the absorption due to uncomplexed Co(II) ($\varepsilon_{512\ nm}$ = 6.0 $m^{-1}{\cdot}cm^{-1}$) [22]. Low-temperature EPR spectroscopy was performed using either a Bruker ESP-300E or a Bruker EleXsys spectrometer equipped with an ER 4116 DM dual mode X-band cavity and an Oxford Instruments ESR-900 helium flow cryostat. Background spectra recorded on a buffer sample were aligned with and subtracted from experimental spectra as in earlier work [33,50]. EPR spectra were recorded at microwave frequencies of approximately 9.65 GHz: precise microwave frequencies were recorded for individual spectra to ensure precise *g*-alignment. All spectra were recorded at 100 kHz modulation frequency. Other EPR running parameters are specified in the figure legends for individual samples. EPR simulations were carried out using matrix diagonalization (xsophe, Bruker Biospin), assuming a spin Hamiltonian $H = \beta g HS + SDS + SAI$, with $S = 3/2$ and $D > \beta g HS$ (= $h\nu$). Enzyme concentrations for EPR were 1 mm. Mutated enzyme samples for EPR were frozen after incubation with the appropriate amount of Co(II) for 60 min at 25 °C.

FEBS Journal, Vol. 275, No. 24 (December 2008): pg. 6248-6259. DOI.

Acknowledgements

This work was supported by the National Science Foundation (CHE-0652981, R. C. Holz) and the National Institutes of Health (AI056231, B. Bennett). The Bruker Elexsys spectrometer was purchased by the Medical College of Wisconsin and is supported with funds from the National Institutes of Health (NIH, EB001980, B. Bennett).

Abbreviations

*Ec*MetAP-I	type I methionine aminopeptidase from *Escherichia coli*
eq.	equivalent
EXAFS	extended X-ray absorption fine structure spectroscopy
ICP-AES	inductively coupled plasma–atomic emission spectroscopy
ITC	isothermal calorimetry
MCD	magnetic CD
MGMM	Met-Gly-Met-Met
*Pf*MetAP-II	type II methionine aminopeptidase from *Pyrococcus furiosus*

References

1. Bradshaw RA. Protein translocation and turnover in eukaryotic cells. TIBS. 1989;14:276–279.
2. Meinnel T, Mechulam Y, Blanquet S. Methionine as translation start signal – a review of the enzymes of the pathway in *Escherichia coli*. Biochimie. 1993;75:1061–1075.
3. Bradshaw RA, Brickey WW, Walker KW. N-terminal processing: the methionine aminopeptidase and N^{α}-acetyl transferase families. TIBS. 1998;23:263–267.
4. Arfin SM, Bradshaw RA. Cotranslational processing and protein turnover in eukaryotic cells. Biochemistry. 1988;27:7979–7984.
5. Lowther WT, Matthews BW. Metalloamino-peptidases: common functional themes in disparate structural surroundings. Chem Rev. 2002;102:4581–4607.
6. Lowther WT, Matthews BW. Structure and function of the methionine aminopeptidases. Biochim Biophys Acta. 2000;1477:157–167.
7. Chang S-YP, McGary EC, Chang S. Methionine aminopeptidase gene of *Escherichia coli* is essential for cell growth. J Bacteriol. 1989;171:4071–4072.

8. Chang Y-H, Teichert U, Smith JA. Molecular cloning, sequencing, deletion, and overexpression of a methionine aminopeptidase gene from *Saccharomyces cerevisiae*. J Biol Chem. 1992;267:8007–8011.
9. Li X, Chang Y-H. Amino terminal protein processing in *Saccharomyces cerevisiae* is an essential function that requires two distinct methionine aminopeptidases. Proc Natl Acad Sci USA. 1995;92:12357–12361
10. Miller CG, Kukral AM, Miller JL, Movva NR. *pepM* is an essential gene in *Salmonella typhimurium*. J Bacteriol. 1989;171:5215–5217.
11. Taunton J. How to starve a tumor. Chem Biol. 1997;4:493–496.
12. Griffith EC, Su Z, Turk BE, Chen S, Chang Y-H, Wu Z, Biemann K, Liu JO. Methionine aminopeptidase (type 2) is the common target for angiogenesis inhibitors AGM-1470 and ovalicin. Chem Biol. 1997;4:461–471.
13. Sin N, Meng L, Wang MQ, Wen JJ, Bornmann WG, Crews CM. The anti-angiogenic agent fumagillin covalently binds and inhibits the methionine aminopeptidase, MetAP-2. Proc Natl Acad Sci USA. 1997;94:6099–6103.
14. Liu S, Widom J, Kemp CW, Crews CM, Clardy J. Structure of the human methionine aminopeptidase-2 complexed with fumagillin. Science. 1998;282:1324–1327.
15. Lowther WT, McMillen DA, Orville AM, Matthews BW. The anti-angiogenic agent fumagillin covalently modifies a conserved active site histidine in the *Escherichia coli* methionine aminopeptidase. Proc Natl Acad Sci USA. 1998;95:12153–12157.
16. Douangamath A, Dale GE, D'Arcy A, Almstetter M, Eckl R, Frutos-Hoener A, Henkel B, Illgen K, Nerdinger S, Schulz H, et al. Crystal structures of *Staphylococcus aureus* methionine aminopeptidase complexed with keto heterocycle and aminoketone inhibitors reveal the formation of a tetrahedral intermediate. J Med Chem. 2004;47:1325–1328.
17. Tahirov TH, Oki H, Tsukihara T, Ogasahara K, Yutani K, Ogata K, Izu Y, Tsunasawa S, Kato I. Crystal structure of the methionine aminopeptidase from the hyperthermophile, *Pyrococcus furiosus*. J Mol Biol. 1998;284:101–124.
18. Lowther WT, Orville AM, Madden DT, Lim S, Rich DH, Matthews BW. *Escherichia coli* methionine aminopeptidase: implications of crystallographic analyses of the native, mutant and inhibited enzymes for the mechanism of catalysis. Biochemistry. 1999;38:7678–7688.
19. Roderick LS, Matthews BW. Structure of the cobalt-dependent methionine aminopeptidase from *Escherichia coli*: a new type of proteolytic enzyme. Biochemistry. 1993;32:3907–3912.
20. Spraggon G, Schwarzenbacher R, Kreusch A, McMullan D, Brinen LS, Canaves JM, Dai X, Deacon AM, Elsliger MA, Eshagi S, et al. Crystal

structure of a methionine aminopeptidase (TM1478) from *Thermotoga maritima* at 1.9 Å resolution. Proteins. 2004;56:396–400.
21. Addlagatta A, Hu X, Liu JO, Matthews BW. Structural basis for the functional differences between type I and type II human methionine aminopeptidases. Biochemistry. 2005;44:14741–14749.
22. D'Souza VM, Bennett B, Copik AJ, Holz RC. Characterization of the divalent metal binding properties of the methionyl aminopeptidase from *Escherichia coli*. Biochemistry. 2000;39:3817–3826.
23. Cosper NJ, D'Souza V, Scott R, Holz RC. Structural evidence that the methionyl aminopeptidase from *Escherichia coli* is a mononuclear metalloprotease. Biochemistry. 2001;40:13302–13309.
24. Ye QZ, Xie SX, Ma ZQ, Huang M, Hanzlik RP. Structural basis of catalysis by monometalated methionine aminopeptidase. Proc Natl Acad Sci USA. 2006;103:9470–9475.
25. Meng L, Ruebush S, D'Souza VM, Copik AJ, Tsunasawa S, Holz RC. Overexpression and divalent metal binding studies for the methionyl aminopeptidase from *Pyrococcus furiosus*. Biochemistry. 2002;41:7199–7208.
26. Larrabee JA, Leung CH, Moore R, Thamrong-nawasawat T, Wessler BH. Magnetic circular dichroism and cobalt(II) binding equilibrium studies of Escherichia coli methionyl aminopeptidase. J Am Chem Soc. 2004;126:12316–12324.
27. Wang J, Sheppard GS, Lou P, Kawai M, Park C, Egan DA, Schneider A, Bouska J, Lesniewski R, Henkin J. Physiologically relevant metal cofactor for methionine aminopeptidase-2 is manganese. Biochemistry. 2003;42:5035–5042.
28. Hu XV, Chen X, Han KC, Mildvan AS, Liu JO. Kinetic and mutational studies of the number of interacting divalent cations required by bacterial and human methionine aminopeptidases. Biochemistry. 2007;46:12833–12843.
29. Copik AJ, Nocek B, Swierczek SI, Ruebush S, SeBok J, D'Souza VM, Peters J, Bennett B, Holz RC. EPR and X-ray crystallographic characterization of the product bound form of the Mn(II)-loaded methionyl aminopeptidase from Pyrococcus furiosus. Biochemistry. 2005;44:121–129.
30. D'Souza VM, Brown RS, Bennett B, Holz RC. Charaterization of the active site and insight into the binding mode of the anti-angiogenesis agent fumagillin to the Mn(II)-loaded methionyl aminopeptidase from Escherichia coli. J Biol Inorg Chem. 2005;10:41–50.
31. D'Souza VM, Holz RC. The methionyl aminopeptidase from *Escherichia coli* is an iron(II) containing enzyme. Biochemistry. 1999;38:11079–11085.

32. Winzor DJ, Sawyer WH. Quantitative Characterization of Ligand Binding. New York, NY: Wiley-Liss; 1995.
33. Bennett B, Holz RC. EPR studies on the mono- and dicobalt(II)-substituted forms of the aminopeptidase from *Aeromonas proteolytica*. Insight into the catalytic mechanism of dinuclear hydrolases. J Am Chem Soc. 1997;119:1923–1933.
34. Huntington KM, Bienvenue D, Wei Y, Bennett B, Holz RC, Pei D. Slow-binding inhibition of the aminopeptidase from *Aeromonas proteolytica* by peptide thiols: synthesis and spectral characterization. Biochemistry. 1999;38:15587–15596.
35. Bienvenue D, Bennett B, Holz RC. Inhibition of the aminopeptidase from *Aeromonas proteolytica* by L-leucinethiol: kinetic and spectroscopic characterization of a slow, tight-binding inhibitor–enzyme complex. J Inorg Biochem. 2000;78:43–54.
36. Crawford PA, Yang K-W, Sharma N, Bennett B, Crowder MW. Spectroscopic studies on cobalt(II)-substituted metallo-β-lactamase ImiS from *Aeromonas veronii bv sobria*. Biochemistry. 2005;44:5168–5176.
37. Vallee BL, Auld DS. Cocatalytic zinc motifs in enzyme catalysis. Proc Natl Acad Sci USA. 1993;90:2715–2718.
38. Vallee BL, Auld DS. New perspective on zinc biochemistry: cocatalytic sites in multi-zinc enzymes. Biochemistry. 1993;32:6493–6500.
39. Lipscomb WN, Sträter N. Recent advances in zinc enzymology. Chem Rev. 1996;96:2375–2433.
40. Dismukes GC. Manganese enzymes with binuclear active sites. Chem Rev. 1996;96:2909–2926.
41. Sträter N, Lipscomb WN, Klabunde T, Krebs B. Two-metal ion catalysis in enzymatic acyl- and phosphoryl-transfer reactions. Angew Chem Int Ed Engl. 1996;35:2024–2055.
42. Wilcox DE. Binuclear metallohydrolases. Chem Rev. 1996;96:2435–2458.
43. Bazan JF, Weaver LH, Roderick SL, Huber R, Matthews BW. Sequence and structure comparison suggest that methionine aminopeptidase, prolidase, aminopeptidase-P, and creatinase share a common fold. Proc Natl Acad Sci USA. 1994;91:2473–2477.
44. Oefner C, Douangamath A, D'Arcy AHS, Mareque D, MacSweeney A, Padilla J, Pierau S, Schulz H, Thormann M, Wadman S, et al. The 1.15 Å crystal structure of the *Staphylococcus aureus* methionyl aminopeptidase and complexes with triazole based inhibitors. J Mol Biol. 2003;332:13–21.
45. Maher MJ, Ghosh M, Grunden AM, Menon AL, Adams MW, Freeman HC, Guss JM. Structure of the prolidase from *Pyrococcus furiosus*. Biochemistry. 2004;43:2771–2783.

46. Wilce MCJ, Bond CS, Dixon NE, Freeman HC, Guss JM, Lilley PE, Wilce JA. Structure and mechanism of a proline-specific aminopeptidase from *Escherichia coli*. Proc Natl Acad Sci USA. 1998;95:3472–3477.
47. Chiu C-H, Lee C-Z, Lin K-S, Tam MF, Lin L-Y. Amino acid residues involved in the functional integrity of the *Escherichia coli* methionine aminopeptidase. J Bacteriol. 1999;181:4686–4689.
48. Bertini I, Luchinat C. High-spin cobalt(II) as a probe for the investigation of metalloproteins. Adv Inorg Biochem. 1984;6:71–111.
49. Copik AJ, Swierczek SI, Lowther WT, D'Souza V, Matthews BW, Holz RC. Kinetic and spectroscopic characterization of the H178A mutant of the methionyl aminopeptidase from *Escherichia coli*. Biochemistry. 2003;42:6283–6292.
50. Bennett B, Holz RC. Spectroscopically distinct cobalt(II) sites in heterodimetallic forms of the aminopeptidase from *Aeromonas proteolytica*: characterization of substrate binding. Biochemistry. 1997;36:9837–9846.